JACS
JOURNAL OF THE AMERICAN CHEMICAL SOCIETY
Article
pubs.acs.org/JACS

Platinum Nanoparticles on Gallium Nitride Surfaces: Effect of Semiconductor Doping on Nanoparticle Reactivity

Susanne Schäfer,[†] Sonja A. Wyrzgol,[‡] Roberta Caterino,[†] Andreas Jentys,[‡] Sebastian J. Schoell,[†] Michael Hävecker,[∥] Axel Knop-Gericke,[∥] Johannes A. Lercher,*[,‡] Ian D. Sharp,[†,§] and Martin Stutzmann*[,†,‡]

[†]Walter Schottky Institut, Technische Universität München, Am Coulombwall 4, 85748 Garching, Germany
[‡]Catalysis Research Center, Technische Universität München, Lichtenbergstrasse 4, 85747 Garching, Germany
[∥]Fritz-Haber-Institut der Max-Planck-Gesellschaft, Department of Inorganic Chemistry, Faradayweg 4-6, 14195 Berlin, Germany

Supporting Information

ABSTRACT: Platinum nanoparticles supported on n- and p-type gallium nitride (GaN) are investigated as novel hybrid systems for the electronic control of catalytic activity via electronic interactions with the semiconductor support. *In situ* oxidation and reduction were studied with high pressure photoemission spectroscopy. The experiments revealed that the underlying wide-band-gap semiconductor has a large influence on the chemical composition and oxygen affinity of supported nanoparticles under X-ray irradiation. For as-deposited Pt cuboctahedra supported on n-type GaN, a higher fraction of oxidized surface atoms was observed compared to cuboctahedral particles supported on p-type GaN. Under an oxygen atmosphere, immediate oxidation was recorded for nanoparticles on n-type GaN, whereas little oxidation was observed for nanoparticles on p-type GaN. Together, these results indicate that changes in the Pt chemical state under X-ray irradiation depend on the type of GaN doping. The strong interaction between the nanoparticles and the support is consistent with charge transfer of X-ray photogenerated free carriers at the semiconductor−nanoparticle interface and suggests that GaN is a promising wide-band-gap support material for photocatalysis and electronic control of catalysis.

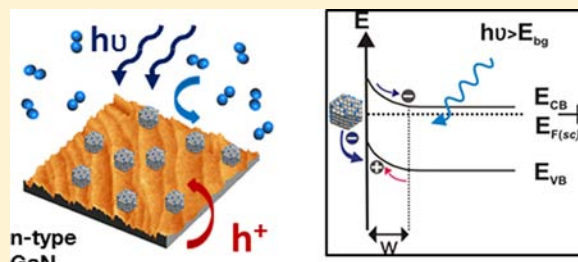

1. INTRODUCTION

A key challenge in the knowledge-guided synthesis of photocatalytic systems is to couple photon energy into a catalytically active species via selective charge transfer and to use this input to modify catalytic activity and selectivity. Such control conceptually requires the use of semiconductor support materials in combination with supported metal nanoparticles. Progress in that respect would yield advanced concepts for energy conversion and storage as well as the development of energy and resource efficient catalysts (green chemistry). As supported catalysts are used in a wide range of reactions, numerous studies have been devoted to understand and, at least partly, control the properties of metal nanoparticles affecting their catalytic performance. Nanoparticles tuned in shape and size have been used to investigate activity and selectivity in multipath reactions.[1−5] Metal−support interactions have been described for several oxides.[6,7] Croy et al. investigated MeOH decomposition by Pt nanoparticles supported on reducible (CeO_2, TiO_2) and nonreducible (SiO_2, ZrO_2, Al_2O_3) oxide powders, with the highest activity obtained on ZrO_2 supports.[8] Moreover, the formation and stability of Pt oxides on Pt nanoparticles was investigated for SiO_2, TiO_2, and ZrO_2 supports. Only a weak interaction was obtained for SiO_2, while nanoparticle flattening occurred on ZrO_2. Probably the best known example for a strong metal−support interaction is TiO_2, on which particle encapsulation was observed after annealing at temperatures above 1273 K.[9] Although some oxidic supports exhibit semiconducting properties, the influence and potential impact of an underlying semiconductor are rarely discussed. For applications in photocatalysis, extensive studies were performed on the wide-band-gap semiconductors TiO_2 and ZnO. In terms of band gap and band position at the surface, these materials are similar to GaN. Consequently, both GaN and TiO_2 have been investigated as candidates for water splitting or light harvesting.[10−13] However, metal oxides such as ZnO and TiO_2 exhibit a high background n-type conductivity, and consequently, p-type doping remains difficult for these oxide materials. In contrast, GaN is one of the few wide-band-gap semiconductors (E_G = 3.4 eV) that is available with controlled, electronic n- and p-type doping. With the Pt work function being located approximately in the middle of the GaN band gap (5.6 eV), GaN/Pt hybrid structures provide a rare combination for the investigation of the dependence of charge transfer on the semiconductor doping (Supporting Information (SI): Figure S 1). The GaN surface charge density can be

Received: February 29, 2012
Published: June 27, 2012

© 2012 American Chemical Society

adjusted by thermal, electrical, or optical means. Therefore, it may be possible to utilize GaN substrates as electronically active supports which influence the catalytic activity of nanoparticles on the surface.

GaN is a thermally and chemically stable material, and decomposition is not observed up to temperatures above 1100 K.[14] Typically, a thin layer of oxygen is observed on the GaN surface when it is exposed to atmosphere at room temperature.[15−17] For ordered GaN (0001), oxygen saturation coverages have been determined experimentally to be between 0.4 ML[18] and 0.9 ML.[19] According to Zywietz et al., the adsorption of oxygen on GaN (0001) is exothermic for coverages up to 0.8 ML.[20] Both experiments and theoretical calculations verify oxygen binding only to the Ga atoms; bond formation to nitrogen atoms has not been observed. The formation of an intermediate gallium oxide species (GaO_X) was reported to occur prior to the formation of the stoichiometric Ga_2O_3. Although oxygen is always present on GaN surfaces, an electrically insulating oxide layer can only be grown at temperatures above 975 K.[21,22]

In recent years, Pt-GaN compounds have been used as Schottky diodes for the detection of small molecules such as hydrogen.[23] Furthermore, the detection of a hot electron chemicurrent was shown for nanoscale Schottky diodes upon the exothermic oxidation of CO to CO_2.[24] The surface band bending, which is determined by the Fermi level alignment of the metal and the semiconductor, provides the intrinsic electric field for the separation of photogenerated electron−hole pairs and the driving force of free carriers to the interface (Figure 4). However, the nanoscale metal−semiconductor interface is complex, and both nanoparticle and semiconductor properties must be considered in order to understand chemical and electronic interactions at the interface. The direct comparison of Pt nanoparticles on electronically active n- and p-type GaN supports allows discrimination of photoinduced charge transfer from other energy dissipation channels, such as hot electron generation on the Pt surface or phonon generation.

Recent preliminary experiments in our laboratory have provided evidence that the catalytic performance of Pt nanoparticles can be electronically controlled via light stimulation by using n- and p-type GaN supports (a detailed kinetic study is in preparation). Ethene hydrogenation to ethane was used as a test reaction in a recycle reactor with a UV-transparent quartz glass window. Under above-band-gap illumination (254 nm), the Pt reactivity was significantly altered. While the conversion rate decreased for Pt cuboctahedra on n-type GaN upon illumination, the rate was enhanced for p-type GaN. The differences in conversion rate under illumination and in darkness are consistent with photoinduced charge transfer. Based on these observations, we have performed a comparative study on the interactions between Pt nanoparticles and n- and p-type GaN surfaces. The distributions and coverages of spin-coated Pt cuboctahedra on GaN are analyzed with transmission electron microscopy (TEM) and atomic force microscopy (AFM). *In situ* high pressure XPS provides a suitable method to characterize the Pt-GaN system, under both photoexcitation and reaction conditions. The chemical compositions of the nanoparticles and the underlying supports are discussed in terms of the semiconductor band alignment, where effects on the chemical properties are tested by *in situ* reduction and oxidation experiments. A model for charge transfer under synchrotron radiation is presented, elucidating the observed differences of the Pt oxidation behavior on n-type and p-type GaN supports. Considerations of the GaN/Pt nanoparticle material system are highly relevant for other semiconductor−nanoparticle compounds used in (photo)catalysis.

2. EXPERIMENTAL SECTION

2.1. Sample Preparation. Shape selective, monodisperse Pt nanoparticles were prepared by the polyol process using silver nitrate to achieve cuboctahedral nanoparticles.[2,25] Polyvinylpyrrolidone (PVP) was used as the protecting shell to avoid clustering in solution.[25] The average particle size in ethanol was 8.1 nm, as determined by TEM measurements (JEOL 2010) (Figure 1a).

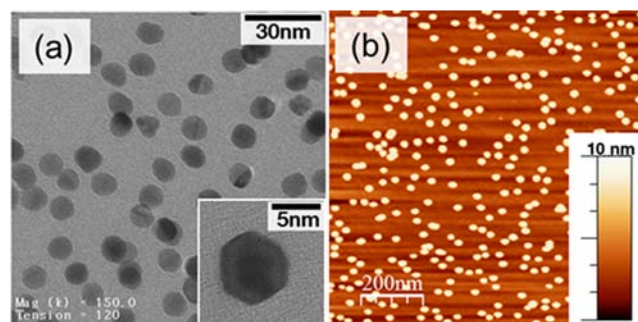

Figure 1. Monodisperse Pt cuboctahedra deposited on a TEM grid (TEM, a) and deposited on n-type GaN (AFM, b).

MOCVD-grown GaN thin films (3 μm) were used as nanoparticle support, with net carrier concentrations (300 K) of $n = 2 \times 10^{18}$ cm^{-3} for n-type, and $p = 5 \times 10^{17}$ cm^{-3} for p-type GaN. MOCVD-grown GaN exhibits Ga-face crystal polarity along the [0001] axis, resulting in high mechanical and chemical stability due to low surface defect concentrations.[26−28] To avoid sample charging during photoemission experiments, ohmic contacts were evaporated onto the edges of all GaN samples (n-type GaN: Ti/Al 30/70 nm; p-type GaN: Ni/Au 20/20 nm)[29,30] and annealed at 775 K for 5 min prior to nanoparticle deposition. The surface morphologies of the annealed reference samples were characterized by AFM, revealing smooth surfaces with atomic growth steps (SI: Figure S3). All substrates were cleaned in acetone (ultrasonic bath, 10 min) and rinsed with 2-propanol (5 min). After cleaning, a defined Pt dispersion (2.2×10^{-3} mol L^{-1} Pt in ethanol) was pipetted onto the GaN surfaces and spincoated at 3000 rpm for 60 s. Excess solvent was removed by heating the samples to 360 K for 5 min. The remaining PVP-capping was stripped by oxygen plasma treatment with an oxygen pressure of 1.4 mbar at 200 W for 5 min (TePla 100-E, Technics Plasma GmbH). To increase the adhesive forces between particles and GaN surfaces, the samples were moderately heated to 425 K for 15 min in 100 mbar N_2.[31,32] The complete removal of PVP fragments after oxygen plasma treatment was verified by the absence of any peaks related to organic fragments in thermal desorption spectra up to 800 K (SI: Figure S2). The distribution of the deposited nanoparticles on GaN surfaces was characterized by AFM (Veeco Multimode, Nanoscope V) in tapping mode (Figure 1b). The average number of particles per cm^2 was used to calculate the total number of Pt atoms on the sample and the fraction of surface atoms, reported in %ML, with respect to an atom density of 1.5×10^{15} cm^{-2} for Pt(111). It was assumed that the deposited nanoparticles are truncated and only two-thirds of the surface atoms contribute to the chemically active surface area, while one-third is in direct contact with the support. The number of Pt atoms per particle as well as the number of Pt surface atoms was calculated assuming 15 atomic shells around a single atom inside the cuboctahedron.[33] Two sets of samples were used for the experiments presented in this work. The first set of samples contained as-prepared nanoparticles after oxygen plasma treatment on both n- and p-type GaN. These samples were used for *in situ* reduction. A second set of identical samples was reduced *ex situ* in flowing hydrogen (1 bar, 100

dx.doi.org/10.1021/ja3020132 | J. Am. Chem. Soc. 2012, 134, 12528−12535

mL min^{-1}) at 775 K for 3 h. These samples were stored and transported in nitrogen without exposure to air. *In situ* oxidation was performed with these samples.

2.2. *In Situ* Photoemission Spectroscopy. The *in situ* high-pressure XPS measurements were performed at the ISISS beamline at BESSY II (Helmholtz-Zentrum Berlin). The ISISS setup consists of a loadlock and a high-pressure XPS (HP-XPS) analysis chamber with a base pressure of 1×10^{-7} mbar. A differentially pumped electrostatic lense system was used to maintain a high count rate by reducing photoelectron scattering at high pressures. A sapphire holder was used that allows for laser heating during measurement. Sufficient grounding was ensured by clamping the ohmically contacted samples between two stainless steel plates with optical access to the sample provided by a 3 mm diameter hole in the top plate. The setup is described in more detail by Salmeron and Schlögl and by Knop-Gericke et al.[34,35] For our measurements, the incident monochromatic photon energy was adjusted with respect to the analyzed core level binding energies, resulting in a constant photoelectron kinetic energy of ≈270 eV for all species. Hence, the probed material depth was ≈8 Å for all analyzed species.[36] Detailed spectra were collected for O 1s, N 1s, C 1s, Pt 4f, and Ga 3d core levels. In a first experiment, the effect of the GaN support doping on the oxidation state of the nanoparticles under X-ray irradiation was investigated. Pt 4f core level spectra were acquired from the as-prepared samples in vacuum, in hydrogen at room temperature, and during *in situ* reduction in hydrogen atmosphere at 800 K. In a second experiment using the second set of samples, the *in situ* oxidation of Pt nanoparticles in oxygen atmosphere was investigated. In both experiments, the gas pressure was adjusted to 0.5 mbar using an electronically controlled butterfly valve. The gas flow rates were held constant using mass flow controllers. The quantitative analysis of peak positions, line widths, and relative peak areas was performed using CASA XPS software. A Shirley background was subtracted prior to peak fitting to account for energy loss processes.[37] Asymmetric Doniach–Sunjic functions with small asymmetry factors of 0.008–0.01 were applied to fit the Pt 4f core level spectra (Table 2). Spin–orbit coupling results in a Pt 4f doublet structure with a peak separation of $\Delta = 3.3$ eV and a branching ratio of 0.75 between Pt $4f_{5/2}$ and Pt $4f_{7/2}$. The full width at half-maximum (fwhm) was restricted to 1.0 ± 0.1 eV for all Pt oxidation states. The Pt/Ga element ratio was used as a measure of the total Pt coverage, taking into account the respective peak areas, *A*, the ionization cross sections, σ, and the energy dependent incident photon flux, φ (Table 1) according to the following:

$$\text{Pt/Ga} = \frac{A(\text{Pt 4f})\cdot\sigma_{\text{Ga 3d}}\cdot\varphi_{\text{Ga 3d}}}{A(\text{Ga 3d})\cdot\sigma_{\text{Pt 4f}}\cdot\varphi_{\text{Pt 4f}}} \tag{1}$$

Table 1. Energy Dependent Photon Flux and Ionization Cross Sections for Ga 3d and Pt 4f Core Levels

core level	photon energy (eV)	photon flux (s^{-1})	cross section (b)[48,49]
Ga 3d	285	4.32×10^{10}	2.04
Pt 4f	365	1.72×10^{10}	5.03

3. RESULTS

Spincoating of monodisperse, cuboctahedral nanoparticles onto GaN surfaces provides a highly reproducible, homogeneous, and stable nanoparticle distribution without agglomeration.[31] Although this method does not create ordered arrays of nanoparticles, it is suitable for preparation of low coverage model catalyst systems to study nanoparticle–support interactions. Hence, spincoating provides a good alternative to, for example, Langmuir–Blodgett or physical vapor deposition of catalytic particles.[2] Prior to XPS measurements, the total amount of Pt on the surface was assessed from the nanoparticle diameter (TEM) and the aeral density of nanoparticles (AFM). The total platinum coverage was 16 ± 3%ML (17 ± 5%ML) for cuboctahedra on n-type (p-type) GaN. The fraction of Pt surface atoms was 3.1 ± 0.5%ML (3.2 ± 0.9%ML) for n-type (p-type) GaN. The determined coverages were identical on n-type and p-type GaN within the experimental error (Table 3). The coverages were evaluated independently using AFM and XPS data. Only the surface atoms contribute to the calculated coverage in the case of the AFM data, while the XPS data yields information about all Pt atoms within the photoelectron escape depth of 8 Å. Considering this, the evaluated coverages are in very good agreement. Accordingly, the following discussion applies for Pt atoms at or in close proximity to the nanoparticle surface.

As a first photoemission experiment, the dependence of the chemical composition of the as-prepared Pt nanoparticles at room temperature (RT) in vacuum and in hydrogen was evaluated with respect to the semiconductor doping. For cuboctahedra on n-type GaN, the Pt 4f spectra were deconvoluted into four components (Figure 2a,c). The component with the lowest binding energy (E_B) was assigned to metallic platinum Pt^0 at 71.8 eV (71.4 eV) in vacuum (hydrogen). The three oxidized species Pt^{ox} were located at

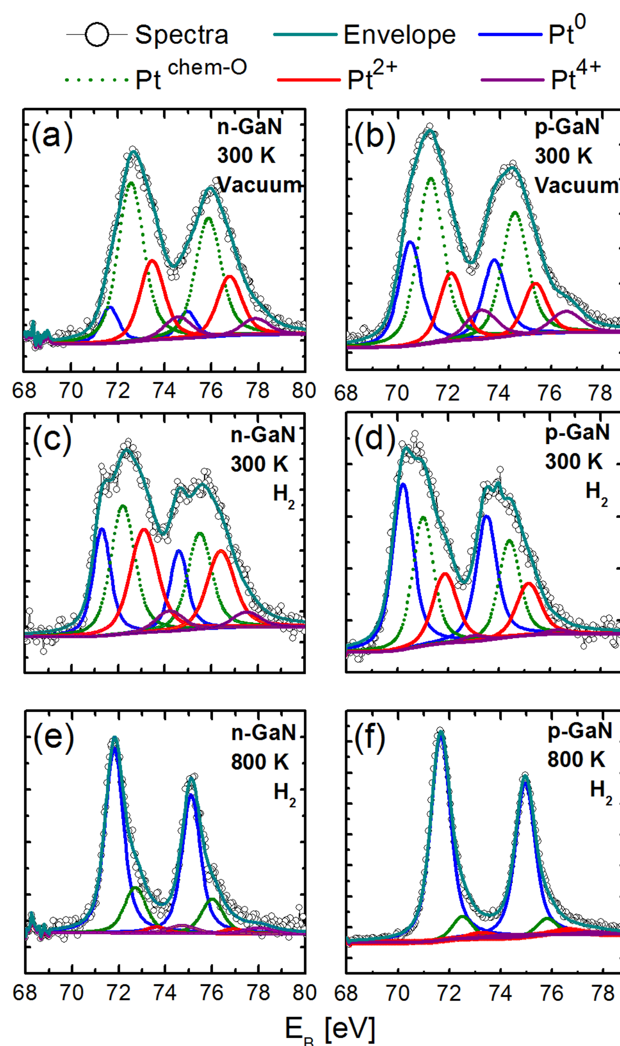

Figure 2. Pt 4f core level spectra of cuboctahedra on n-type (a,c,e) and p-type GaN (b,d,f): before reduction in vacuum at 300 K (a,b) and in hydrogen at 300 K (c,d), and after reduction in hydrogen at 800 K (e,f).

Table 2. Absolute Pt^0 Binding Energies and Relative Shifts for Pt^{ox} Components of As-Prepared Samples and Nanoparticles during *in Situ* Oxidation[a]

substrate	experiment	$E_B(Pt^0)$ (eV)	$CLS(Pt^{chem-O})$ (eV)	$CLS(Pt^{2+})$ (eV)	$CLS(Pt^{4+})$ (eV)
n-type GaN	as-prepared (Vac/H_2)	71.8/71.4	+0.9	+1.8	+2.9
	oxidation	71.3	+1.1	+2.2	+3.7
p-type GaN	as-prepared (Vac/H_2)	70.5/70.1	+0.8	+1.6	+2.8
	oxidation	70.0	+0.8	+1.6	+2.8
Doniach−Sunjic (α,n)		(0.008, 190)	(0.010, 250)	(0.020, 300)	(0.020, 300)

[a]The asymmetry factor, α, and the convolution factor, n, used in the Doniach−Sunjic functions are also given.

core level shifts (CLSs) of +0.9 eV, +1.8 eV, and +2.9 eV with respect to Pt^0 (Table 2). These species were attributed to platinum atoms with chemisorbed oxygen (Pt^{Chem-O}), Pt^{2+}, and Pt^{4+}, respectively.[37−39] The same assignment was applied for deconvolution of the spectra obtained for cuboctahedra on p-type GaN (Figure 2b,d). Interestingly, for the p-type support, the absolute position of the Pt^0 peak was shifted to lower E_B (70.5 eV/70.1 eV in vacuum/hydrogen), and the relative shifts of the Pt^{ox} components were determined to be +0.8 eV, +1.6 eV, and +2.8 eV, respectively. Furthermore, the fraction of Pt^0/Pt^{total} in vacuum was 24% for nanoparticles on p-type, compared to only 12% for n-type GaN. Upon hydrogen inlet, the fraction of Pt^0/Pt^{total} immediately increased to 43% for nanoparticles on p-type GaN, but only to 23% for n-type GaN. In both cases, the Pt 4f spectra for n-type GaN were dominated by the Pt^{Chem-O} and Pt^{2+} species and with a smaller contribution from Pt^{4+}. Generally, for p-type support, the Pt^{Chem-O} and Pt^{2+} components were less pronounced and Pt^{4+} was not observed in hydrogen atmosphere. In an additional experiment, the possibility of beam-induced changes of the Pt composition was investigated over a duration of 5 h by repeated acquisition of Pt 4f spectra from a single location on the sample (see SI). No beam-induced changes were recorded. In summary, the oxygen plasma treatment for PVP removal results in highly oxidized Pt nanoparticles on both n-type and p-type GaN surfaces. Interestingly, the extent of oxidation, as well as the respective CLSs, vary strongly with semiconductor doping and are higher for nanoparticles supported on n-type GaN. The differences in composition are even more pronounced under X-ray illumination in hydrogen atmosphere. These findings suggest that the semiconductor nature of the GaN support plays a noticeable role in the catalyst−support interaction.

In order to gain further insight into the influence of the semiconductor under reaction conditions, *in situ* reduction and oxidation experiments were performed. During reduction of the as-prepared samples in hydrogen (sample set 1), the temperature was increased from RT to 800 K. The spectra obtained after reduction at 800 K revealed a significant decrease of all Pt^{ox} species for both types of semiconductor doping (Figure 2e,f). From the Pt signal, a total of 87% Pt^0 was obtained for nanoparticles on p-type material, while less than 76% Pt^0 was observed on n-type GaN. In both cases, only the Pt^{Chem-O} component contributed to Pt^{ox}, while Pt^{2+} and Pt^{4+} disappeared completely during reduction. No additional Pt 4f components evolved as a result of the thermal treatment. Furthermore, at 800 K, the absolute position of Pt^0 was identical for both support materials. The possibility of particle detachment during the experiment was evaluated by calculation of the Pt/Ga element ratio before and after reduction. For both n- and p-type GaN supports, the total amount of deposited Pt was found to be 6−7% (Table 3), demonstrating that no Pt was lost during the thermal treatment.

Table 3. Pt Surface Coverage as Determined from TEM/AFM Analysis (Total Amount/Surface Atoms), from the Pt/Ga Element Ratio before Reduction at Room Temperature (RT), and after Reduction at 800 K under Hydrogen

sample	Pt[%ML] (TEM/AFM)	Pt/Ga (RT) (%)	Pt/Ga (800 K) (%)	rms (AFM, 5 × 5 μm^2) (Å)
n-type GaN	16 ± 3/ 3.1 ± 0.5	6.3	6.8	2.5
p-type GaN	17 ± 5/ 3.2 ± 0.9	7.1	7.7	7.5

Changes in Pt chemical activity due to a possible charge transfer under X-ray illumination were further investigated in an *in situ* oxidation experiment (Figure 3). The *ex situ* reduced cuboctahedra on n- and p-type GaN (sample set 2) yielded initial Pt^0 fractions of 69% and 78%, respectively. Prior to

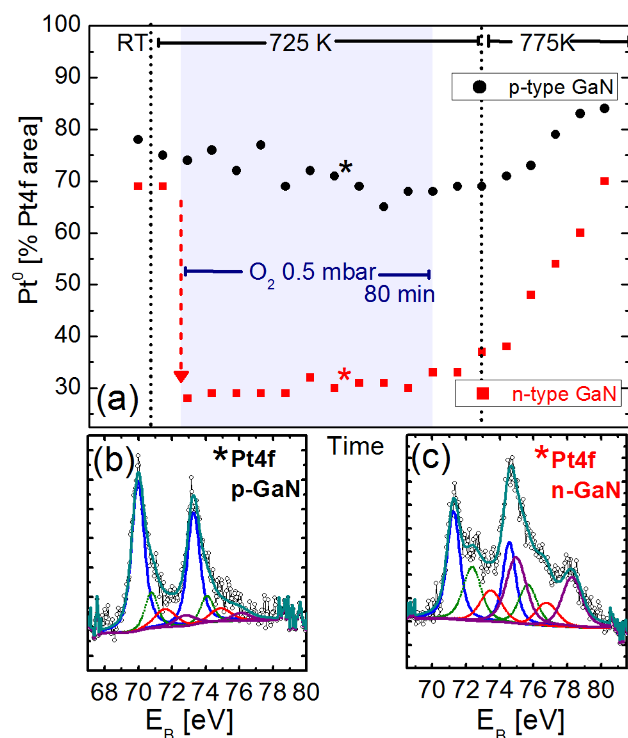

Figure 3. (a) Fraction of Pt^0 as a function of time during oxidation of cuboctahedra on n-type (red squares) and p-type GaN (black circles). Exemplary Pt 4f spectra from p-type (b) and n-type (c) GaN after ≈ 1 h of oxidation (marked by asterisks in part a) are given along with their deconvolution into individual Pt^{ox} components.

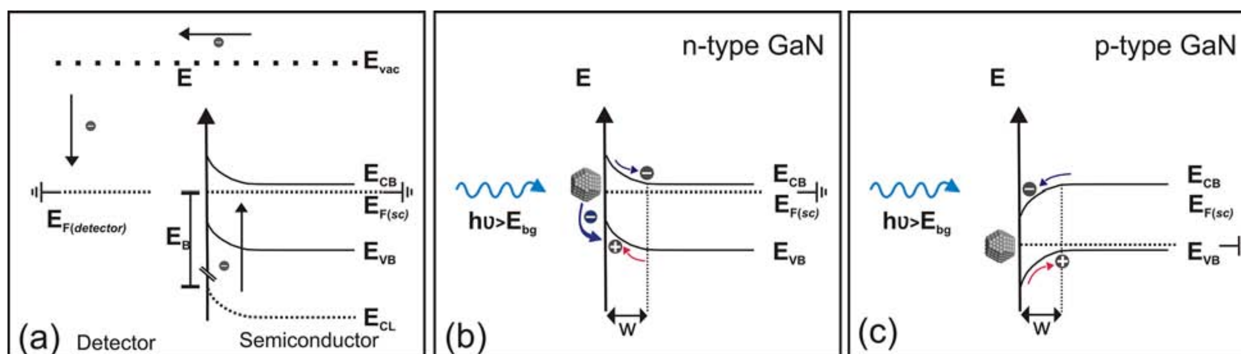

Figure 4. Schematic illustration of the photoelectron detection for an n-type semiconductor (a), where the semiconductor Fermi level, $E_{F(SC)}$, is energetically aligned to the detector ($E_{F(detector)}$). Accordingly, all binding energies, E_B, represent the energy difference between the measured core level, E_{CL}, and the semiconductor Fermi level. Band alignment for Pt particles on GaN and the possible photoinduced charge transfer under X-ray irradiation ($h\nu$) are illustrated for n-type (b) and p-type GaN (c). The semiconductor valence band maximum and conduction band minimum are denoted as E_{VB} and E_{CB}, respectively.

oxygen dosing, the temperature was increased to 725 K. Upon oxygen inlet, only small changes of the Pt 4f composition were recorded for cuboctahedra on p-type GaN in oxygen. Over the course of 80 min of exposure, the amount of Pt^0 decreased to a minimum of 68%. The CLSs of the evolving components relative to Pt^0 were identical to the positions found for as-prepared p-type samples (Table 2). In contrast, the Pt^0 fraction of cuboctahedra on n-type GaN dropped immediately upon oxygen inlet and settled to a value of approximately 30%. Furthermore, the CLSs of the Pt^{ox} components relative to Pt^0 were shifted to higher values compared to those of the as-prepared n-type samples (Table 2). In addition, the Pt^{4+} component was more pronounced on n-type GaN. Although the high pressure caused very low count rates and hence a higher uncertainty in peak fitting, the qualitative differences between Pt 4f spectra on n- and p-type GaN are clearly resolved, as shown in Figure 3. After 80 min of oxygen exposure, the chamber was evacuated again and the substrate temperature was increased to 775 K, which resulted in thermal reduction of the nanoparticles to their initial compositions. Two interesting points arise from this experiment. First, the nanoparticle affinity for oxidation is much higher on n-type than on p-type GaN supports under illumination. Second, the CLSs of Pt^{ox} relative to Pt^0 on n-type GaN are larger for *in situ* oxidation under X-ray irradiation than for oxygen plasma preparation in the absence of X-rays.

4. DISCUSSION

The obtained binding energies for Pt^0 in vacuum (Table 2) are in reasonable agreement with literature values, which range from 70.7 to 71.6 eV. For n-type GaN, a positive shift of the absolute Pt 4f binding energy of +1.3 eV was recorded with respect to the binding energy measured for nanoparticles on p-type GaN (Table 2). This shift can be explained by considering the electronic structure of the semiconductor and the effect of illumination.[40] During XPS measurement of a sufficiently grounded sample, the Fermi level of the semiconductor is referenced to that of the detector (Figure 4a). Consequently, all recorded core level binding energies are measured with respect to the semiconductor Fermi level.[41] This is also true for the deposited nanoparticles, since they are electrically contacted through the semiconductor support. Under equilibrium conditions, the Fermi level of the Pt nanoparticles must align with the Fermi level of the support and the core level energies of Pt would be equal on both n- and p-type GaN in darkness. However, the energetic alignment at the surface under optical (X-ray) excitation of the semiconductor support and, thus, nonequilibrium conditions must be considered (see SI for a detailed description). This creates a different situation for interpretation of CLSs compared to metal foil experiments. Under the steady state conditions established by X-ray illumination, the shifts in absolute Pt 4f binding energies are affected by the surface photovoltage (SPV). On n-type GaN, the absolute Pt binding energy is increased by the magnitude of the SPV, whereas it is decreased on p-type GaN (see SI). Importantly, the magnitude of the surface photovoltage is temperature dependent. At elevated temperatures, the SPV decreases in magnitude and ultimately vanishes.[42] As shown in Figure 2e,f, the observed Pt^0 binding energies on n- and p-type GaN substrates are equal when measured at 800 K, thus confirming that the difference in Pt^0 binding energies on n- and p-type GaN at room temperature is a consequence of SPV under X-ray illumination. Upon hydrogen inlet, an absolute shift in Pt^0 binding energy of −0.4 eV was observed (Table 2). Since this shift of the Pt^0 binding energy was not accompanied by a shift of the N 1s core level, it cannot be caused by the surface photovoltage or altered band bending (data not shown). Accordingly, it is identified as a chemical shift related to hydrogen adsorption on the Pt nanoparticles.

The Pt 4f core level spectra were deconvoluted into four doublets (Figure 2). While the first doublet was attributed to Pt^0, the presence and relative position of the second species were determined from a distinct shoulder in the spectra, even following reduction in hydrogen. We attributed this peak to a chemisorbed oxygen species, Pt^{Chem-O}, due to its CLS of +0.9 eV (n-type GaN) and +0.8 eV (p-type GaN). This assignment is supported by Butcher et. al and Kim et. al, who found CLSs of +0.7 eV and +0.6 eV for chemisorbed oxygen on Pt(110) and Pt(111), respectively.[38,39] Both authors relate the formation of a chemisorbed species to X-ray induced dissociation after controlled oxygen dosing. The same arguments have been used to explain chemisorbed oxygen on Au.[43] However, in our experiments, the chemisorbed species is present prior to oxygen introduction. Hence, we attribute its origin to the oxygen plasma treatment used to remove the PVP capping. The third species, with a CLS of +1.8 eV (n-type GaN) and +1.6 eV (p-type GaN) was assigned to Pt^{2+} in PtO.[38] Finally, the fourth Pt species was identified as Pt^{4+} in PtO_2 with

CLSs of +2.9 eV and +2.8 eV for n-type and p-type GaN, respectively.[37,39] It should be noted that the use of different asymmetry factors could eliminate the fourth doublet. However, the overall background of the spectra does not allow for a higher asymmetry factor. Consequently, we conclude that the fourth species is necessary to obtain an appropriate fit. The magnitudes of the CLSs can differ slightly from literature values due to nanoparticle size and support material effects. Furthermore, the nature of the oxide species that forms is determined by the specific metal facets, as well as structural inhomogeneities such as steps, kinks, and edges of the metal under investigation.[7,44] Thus, the oxidation behavior can strongly depend on the nanoparticle geometry.

As-prepared nanoparticles on n-type GaN in vacuum exhibit a much larger fraction of oxidized species than those on p-type GaN (Figure 2a,b). This effect is even more pronounced in hydrogen atmosphere (Figure 2c,d). Both data sets indicate a stronger binding of oxygen to Pt nanoparticles on n-type compared to p-type material under X-ray illumination. Based on these observations, we conclude that a strong interaction between the Pt nanoparticles and the support exists, which depends on the substrate doping and alters the nanoparticle affinity to oxygen. Based on the homogeneous nanoparticle distribution observed by AFM on both surfaces, it is possible to exclude clustering as the origin of the observed differences. Furthermore, the samples were prepared under identical conditions and only differ in the support doping. However, given the known interactions between nanoparticles and metal oxide supports such as TiO_2, it is necessary to consider the effects of the oxygen bound to the GaN surface. Due to the larger surface roughness (Table 3), a higher oxygen coverage can be expected on p-type compared to n-type GaN (SI Figure S4). However, the oxygen adsorption energy should be very similar on both Ga-polar surfaces. Consequently, only a thin adlayer of bound oxygen, in the range of 0.8 ML, is expected, and efficient tunneling of charge through the adlayer is possible.[20] For nanoparticles on TiO_2, a reduction mechanism has been proposed that is based on X-ray-induced generation of oxygen vacancies and subsequent oxygen spillover from the nanoparticles to the TiO_2 surface.[45,46] An analogous process was excluded to contribute to the observed behavior on GaN, as no beam-induced reduction of the nanoparticles was observed within 5 h.

In order to account for the observed differences on n-type and p-type GaN, we propose a mechanism that considers the semiconductor band alignment at the interface. The Fermi level of platinum (work function 5.6 eV) is located approximately in the middle of the GaN band gap. Furthermore, at the interface, the conduction and valence bands of the semiconductor are bent upward for n-type GaN and downward for p-type GaN due to surface defects and Schottky barrier formation with the metal. As a result of the band alignment, a charge transfer mechanism is plausible and can explain the observed nanoparticle−support interaction. Upon X-ray illumination during measurement, free charge carriers are photogenerated in the space charge region. Due to the interfacial band bending, free holes are driven to the n-type GaN surface, while free electrons accumulate at the p-type GaN surface (Figure 4b,c). With the given energetic alignment, recombination of electrons from the nanoparticles with holes from the n-type semiconductor under illumination is expected. Likewise, electron transfer to the Pt nanoparticles is expected for p-type supports. Such an interfacial charge transfer process would lead to a reduced net charge of Pt nanoparticles on n-type, and an increased net charge on p-type GaN. A similar argument was previously used to explain the photodegradation of organic monolayers on GaN by Howgate et al.[47] Therefore, we propose that the altered chemical properties of the nanoparticles, which depend strongly on the semiconductor doping, are due to this mechanism.

In order to assess the validity of this charge transfer model, *in situ* reduction and oxidation experiments were performed. Following *in situ* reduction, the amount of oxidized Pt species decreased strongly on both n-type and p-type GaN (Figure 2e,f). The PtO and PtO_2 species disappeared entirely and only Pt^{Chem-O} remained. Since no additional peaks evolved during the treatment, Ga−Pt alloying can be excluded. However, a direct comparison of n- and p-type samples reveals a higher fraction of oxidized Pt for nanoparticles on n-type GaN than on p-type GaN after reduction under the same conditions, supporting the mechanism proposed above. MOCVD-grown GaN is thermally stable up to at least 1100 K, and decomposition is not expected at the reduction temperatures used here, which were all below 800 K.[14] However, the oxygen adlayer is slightly reduced by the hydrogen treatment in the case of p-type GaN, while no changes in surface composition are detected for n-type GaN (see SI). In order to investigate a possible nanoparticle detachment due to surface modification under reduction conditions, we evaluated the Pt coverage before and after reduction. As the Pt/Ga element ratio increased slightly following reduction, we conclude that nanoparticle detachment from the surface did not occur throughout reduction (Table 3). We tentatively attribute the slightly larger Pt/GaN ratio to the removal of contaminants during reduction, resulting in an increase of exposed platinum surface area.

Changes in the oxidation properties of the nanoparticles influenced by the semiconductor doping were further investigated by *in situ* oxidation. *Ex situ* reduction of cuboctahedral nanoparticles had yielded a high fraction of Pt^0, with typical differences in composition for n- and p-type supports. Subsequent *in situ* oxidation under X-ray illumination and measurement were conducted simultaneously. Based on the mechanism involving photogenerated charges at the interface, we expect a large difference in reactivity for nanoparticles on n- and p-type GaN. The Pt nanoparticles are immediately oxidized on n-type GaN upon oxygen dosing, while almost no change of the Pt composition was observed for the nanoparticles on p-type GaN (Figure 3). This striking difference between the oxidation behavior of Pt nanoparticles on n-type and p-type GaN supports under illumination is in excellent agreement with the proposed charge transfer mechanism. Within this model, Pt nanoparticles possess fewer electrons on n-type GaN under illumination than on p-type GaN due to the recombination with minority carriers which drift to the GaN surface. Consequently, the n-type supported nanoparticles should exhibit a higher affinity for electronegative oxygen molecules, as is observed experimentally.

5. CONCLUSION

Monodisperse Pt cuboctahedral nanoparticles supported on doped GaN surfaces are shown to be very suitable model systems to explore photostimulated change of chemical properties. *In situ* reduction and oxidation in a high-pressure XPS system revealed a strong doping-dependent nanoparticle−support interaction, which significantly increased the affinity of

metal nanoparticles to oxygen on n-type GaN supports. In particular, Pt nanoparticles consistently exhibit a higher fraction of metal atoms in a higher oxidation state when supported on n-type GaN irradiated with X-rays. Furthermore, *in situ* measurements revealed that high temperature exposure to oxygen under X-ray illumination led to immediate oxidation of the nanoparticles on n-type, but not on p-type, GaN. We propose a model for photoinduced charge transfer across the nanoparticle−semiconductor interface, which involves recombination of minority carriers from n-type GaN with electrons from the Pt particles. This work highlights the impact of semiconductor support materials and suggests that GaN is a promising support for (photo)catalysis.

■ ASSOCIATED CONTENT

Ⓢ Supporting Information

A detailed description of the Pt Fermi level alignment on n- and p-type GaN is provided together with a theoretical explanation of the resulting shifts in all core level binding energies. Thermal desorption spectra and AFM images are given as additional information on the sample preparation process as well as morphology changes due to the hydrogen treatment. Exemplary N 1s, O 1s, Ga 3d core level spectra at RT are presented for n-type and p-type GaN surfaces with deposited Pt cuboctahedra. The composition of the Ga 3d spectra for n- and p-type GaN are listed for as prepared samples after oxygen plasma, after reduction, and during *in situ* oxidation to illustrate the surface composition. Furthermore, data on possible beam damage and carbon deposition during measurement are provided. This material is available free of charge via the Internet at http://pubs.acs.org.

■ AUTHOR INFORMATION

Corresponding Author

Johannes.Lercher@ch.tum.de; stutz@wsi.tum.de

Present Address

[§]Joint Center for Artificial Photosynthesis, Lawrence Berkeley National Laboratory, 1 Cyclotron Rd., Berkeley, CA 94720, USA.

Notes

The authors declare no competing financial interest.

■ ACKNOWLEDGMENTS

We acknowledge the Helmholtz-Zentrum Berlin—Electron storage ring BESSY II for provision of synchrotron radiation at the ISISS beamline and would like to thank Tulio Rocha, Raoul Blume, and Detre Teschner for assistance. The authors thank Peng Jiang of Lawrence Berkeley National Lab for fruitful discussions and Robert Schlögl of Fritz-Haber-Insitut Berlin for insightful comments during the preparation of this manuscript. This work was supported by Deutsche Forschungsgemeinschaft (DFG) through the TUM International Graduate School of Science and Engineering (IGSSE). TEM analysis was performed at the Laboratory of Electron Microscopy, Department of Chemistry, Technische Universität München. I.D.S. and S.J.S. acknowledge support from the Technische Universität München—Institute for Advanced Study, funded by the German Excellence Initiative. R.C. acknowledges support from the EU Marie Curie Initial Training Network (FP7/2009-2013).

■ REFERENCES

(1) Ahmadi, T. S.; Wang, Z. L.; Green, T. C.; Henglein, A.; El-Sayed, M. A. *Science* **1996**, *272*, 1924−1925.

(2) Song, H.; Kim, F.; Connor, S.; Somorjai, G. A.; Yang, P. *J. Phys. Chem. B* **2005**, *109*, 188−193.

(3) Tsung, C.-K.; Kuhn, J. N.; Huang, W.; Aliaga, C.; Hung, L.-I.; Somorjai, G. A.; Yang, P. *J. Am. Chem. Soc.* **2009**, *131*, 5816−5822.

(4) Somorjai, G. A. *Top. Catal.* **2008**, *49*, 126135.

(5) Somorjai, G. A.; Frei, H.; Park, J. Y. *J. Am. Chem. Soc.* **2009**, *131*, 16589−16605.

(6) Freund, H.-J. *Surf. Sci.* **2002**, *500*, 271−299.

(7) Cuenya, B. R. *Thin Solid Films* **2010**, *518*, 3127−3150.

(8) Croy, J.; Mostafa, S.; Liu, J.; Sohn, Y.; Heinrich, H.; Cuenya, B. *Catal. Lett.* **2007**, *119*, 209−216.

(9) Ono, L. K.; Yuan, B.; Heinrich, H.; Cuenya, B. R. *J. Phys. Chem. C* **2010**, *114*, 22119−22133.

(10) Khan, S. U. M.; Al-Shahry, M.; Ingler, W. B. *Science* **2002**, *297*, 2243−2245.

(11) Fujii, K.; Ono, M.; Iwaki, Y.; Sato, K.; Ohkawa, K.; Yao, T. *J. Phys. Chem. C* **2010**, *114*, 22727−22735.

(12) O'Regan, B.; Grätzel, M. *Nature* **1991**, *353*, 737−740.

(13) Kang, B. K.; Song, Y. H.; Kang, S. M.; Choi, Y. C.; Lee, D. K.; Kim, S.-W.; Yoon, D. H. *J. Electrochem. Soc.* **2011**, *158*, H693−H696.

(14) Ambacher, O.; Brandt, M. S.; Dimitrov, R.; Metzger, T.; Stutzmann, M.; Fischer, R. A.; Miehr, A.; Bergmaier, A.; Dollinger, G. *J. Vac. Sci. Technol. B* **1996**, *14*, 3532−3542.

(15) Prabhakaran, K.; Andersson, T. G.; Nozawa, K. *Appl. Phys. Lett.* **1996**, *69*, 3212−3214.

(16) Shalish, I.; Shapira, Y.; Burstein, L.; Salzman, J. *J. Appl. Phys.* **2001**, *89*, 390−395.

(17) Hashizume, T.; Ootomo, S.; Oyama, S.; Konishi, M.; Hasegawa, H. *Papers from the 28th conference on the physics and chemistry of semiconductor interfaces* **2001**, *19*, 1675−1681.

(18) Bermudez, V. M. *J. Appl. Phys.* **1996**, *80*, 1190−1200.

(19) Janzen, O.; Hahn, C.; Mönch, W. *Eur. Phys. J. B* **1999**, *9*, 315−321.

(20) Zywietz, T. K.; Neugebauer, J.; Scheffler, M. *Appl. Phys. Lett.* **1999**, *74*, 1695−1697.

(21) Weidemann, O.; Monroy, E.; Hahn, E.; Stutzmann, M.; Eickhoff, M. *Appl. Phys. Lett.* **2005**, *86*, 083507.

(22) Steinhoff, G. Group III-nitrides for bio- and electrochemical sensors. Ph.D. Thesis, Technische Universität München, 2008.

(23) Schalwig, J.; Müller, G.; Karrer, U.; Eickhoff, M.; Ambacher, O.; Stutzmann, M.; Görgens, L.; Dollinger, G. *Appl. Phys. Lett.* **2002**, *80*, 1222−1224.

(24) Park, J. Y.; Somorjai, G. A. *J. Vac. Sci. Technol. B* **2006**, *24*, 1967−1971.

(25) Busser, G. W.; van Ommen, J. G.; Lercher, J. A. *J. Phys. Chem. B* **1999**, *103*, 1651−1659.

(26) Dhesi, S. S.; Stagarescu, C. B.; Smith, K. E.; Doppalapudi, D.; Singh, R.; Moustakas, T. D. *Phys. Rev. B* **1997**, *56*, 10271−10275.

(27) Stutzmann, M.; Ambacher, O.; Eickhoff, M.; Karrer, U.; Lima Pimenta, A.; Neuberger, R.; Schalwig, J.; Dimitrov; Schuck, P.; Grober, R. *Phys. Status Solidi (b)* **2001**, *228*, 505−512.

(28) Kowalski, B. J.; Iwanowski, R. J.; Sadowski, J.; Kanski, J.; Grzegory, I.; Porowski, S. *Surf. Sci.* **2002**, *507−510*, 186−191.

(29) Ho, J.-K.; Jong, C.-S.; Chiu, C. C.; Huang, C.-N.; Chen, C.-Y.; Shih, K.-K. *Appl. Phys. Lett.* **1999**, *74*, 1275−1277.

(30) Qiao, D.; Guan, Z. F.; Carlton, J.; Lau, S. S.; Sullivan, G. J. *Appl. Phys. Lett.* **1999**, *74*, 2652−2654.

(31) Schäfer, S.; Wyrzgol, S. A.; Wang, Y.; Lercher, J. A.; Stutzmann, M. *Phys. Status Solidi (c)* **2010**, *7*, 411−414.

(32) Wyrzgol, S. A.; Schafer, S.; Lee, S.; Lee, B.; Vece, M. D.; Li, X.; Seifert, S.; Winans, R. E.; Stutzmann, M.; Lercher, J. A.; Vajda, S. *Phys. Chem. Chem. Phys.* **2010**, *12*, 5585−5595.

(33) Benfield, R. E. *J. Chem. Soc., Faraday Trans.* **1992**, *88*, 1107−1110.

(34) Salmeron, M.; Schlögl, R. *Surf. Sci. Rep.* **2008**, *63*, 31.

(35) Knop-Gericke, A.; Kleimenov, E.; Hävecker, M.; Blume, R.; Teschner, D.; Zafeiratos, S.; Schlögl, R.; Bukhtiyarov, V. I.; Kaichev, V. V.; Prosvirin, I. P.; Nizovskii, A. I.; Bluhm, H.; Barinov, A.; Dudin, P.; Kiskinova, M. In Chapter 4 *X-Ray Photoelectron Spectroscopy for Investigation of Heterogeneous Catalytic Processes*; Gates, B. C., Knözinger, H., Eds.; Academic Press: 2009; Vol. *52*; pp 213−272.
(36) Seah, M. P.; Dench, W. A. *Surf. Interface Anal.* **1979**, *1*, 2−11.
(37) Ono, L. K.; Croy, J. R.; Heinrich, H.; RoldanCuenya, B. *J. Phys. Chem. C* **2011**, *115*, 16856−16866.
(38) Kim, Y. S.; Bostwick, A.; Rotenberg, E.; Ross, P. N.; Hong, S. C.; Mun, B. S. *J. Chem. Phys.* **2010**, *133*, 034501.
(39) Butcher, D. R.; Grass, M. E.; Zeng, Z.; Aksoy, F.; Bluhm, H.; Li, W.-X.; Mun, B. S.; Somorjai, G. A.; Liu, Z. *J. Am. Chem. Soc.* **2011**, *133*, 20319−20325.
(40) Sze, S.; Ng., K. K. *Physics of Semiconductor Devices*, 3rd ed.; Wiley: 2007; p 815.
(41) Ecke, G.; Niebelschütz, M.; Kosiba, R.; Rossow, U.; Cimalla, V.; Liday, J.; Vogriňcic, P.; Pezoldt, J.; Lebedev, V.; Ambacher, O. *J. Electr. Eng.* **2006**, *57*, 354−359.
(42) Long, J. P.; Bermudez, V. M. *Phys. Rev. B* **2002**, *66*, 121308.
(43) Gottfried, J. M.; Schmidt, K. J.; Schroeder, S. L. M.; Christmann, K. *Surf. Sci.* **2002**, *511*, 65−82.
(44) Seriani, N.; Mittendorfer, F. *J. Phys.: Condensed Matter* **2008**, *20*, 184023−184034.
(45) Ono, L. K.; RoldanCuenya, B. *J. Phys. Chem. C* **2008**, *112*, 4676−4686.
(46) Jiang, P.; Porsgaard, S.; Borondics, F.; Köber, M.; Caballero, A.; Bluhm, H.; Besenbacher, F.; Salmeron, M. *J. Am. Chem. Soc.* **2010**, *132*, 2858−2859.
(47) Howgate, J.; Schoell, S. J.; Hoeb, M.; Steins, W.; Baur, B.; Hertrich, S.; Nickel, B.; Sharp, I. D.; Stutzmann, M.; Eickhoff, M. *Adv. Mater.* **2010**, *22*, 2632−2636.
(48) Yeh, J.; Lindau, I. *At. Data Nucl. Data Tables* **1985**, *32*, 1−155.
(49) Yeh, J. *Atomic Calculation of Photoionization Cross-Sections and Asymmetry Parameters*; Routledge: 1993.